Characteristic Assessment of Three-Dimensional Point Clouds in HARDI Using Morphological Metrics

CHANGYU SUN[1,2], CHUNYU CHU[2] , FENG YANG[3], WANYU LIU[2] , ISABELLE E. MAGNIN[1,2], YUEMIN ZHU[1,2]

[1] CREATIS; CNRS UMR 5220; INSERM U1044; INSA Lyon; University of Lyon, France.
502, Bâtiment Blaise Pascal, 7 Avenue Jean Capelle, 69100 Villeurbanne, France
[2] CNRS LIA Metislab, Harbin Institute of Technology, Harbin, China.
[3] School of Computer and Information Technology, Beijing JiaoTong University, Beijing, China.

Résumé - Les nuages tridimensionnels (3D) de points tels que la fonction d'orientation de distribution (ODF) sont largement utilisés pour résoudre les problèmes de croisement de fibres en imagerie de diffusion à haute résolution angulaire (high angular resolution diffusion imaging— HARDI). L'évaluation des caractéristiques ou de la qualité des nuages de points 3D s'effectue le plus souvent en utilisant le critère visuel, bien que l'utilisation de quelques mesures objectives de la qualité soit également réalisée, mesures qui sont directement empruntées de la théorie classique du traitement du signal et de l'image, parce qu'elles sont simples et intuitives à calculer. Cependant, ces mesures ne sont pas toujours pertinentes pour caractériser les nuages de points 3D. Nous proposons un nouveau paradigme pour évaluer les caractéristiques des nuages de points 3D, basé sur la mesure des caractéristiques morphologiques de ces derniers. L'idée consiste à projeter le nuage de points 3D sur un plan angle-distance (ADM), construire une matrice angle-distance (ADMAT), et calculer des paramètres tels que le rapport de longueur, la séparabilité et l'incertitude. Trois méthodes HARDI sont comparées en utilisant les mesures proposées. Les résultats obtenus montrent que les caractéristiques des nuages de points 3D peuvent être évaluées d'une manière relativement complète et quantitative.

Abstract - Three-dimensional (3D) point clouds such as orientation distribution function (ODF) are widely used to resolve fiber crossing problems in high angular resolution diffusion imaging (HARDI). The assessment of 3D point cloud characteristics or quality is addressed most commonly using visual criterion, although the use of a few objective quality metrics is also reported that are directly borrowed from classical signal and image processing theory, because they are intuitive and simple to compute. However, they are not always pertinent to characterize 3D point clouds. We propose a new paradigm to assess 3D point cloud characteristics based on the measurement of the morphological characteristics of 3D point clouds. The idea consists in projecting a 3D point cloud onto an angle-distance map (ADM), constructing an angle-distance matrix (ADMAT), and calculating metrics such as length ratio, separability and uncertainty. The results show that the characteristics of 3D point clouds can be well assessed in a relatively complete and quantitative manner.

1 Introduction

The orientation distribution function (ODF) [1] is a quantity used to describe the orientation architecture of the tissue's fibers or fiber bundles; it gives the probability of diffusion in different directions. ODF is often estimated or reconstructed from high angular resolution diffusion imaging (HARDI) such as q-ball imaging (QBI) [2] using spherical sampling. In this field, most existing works put emphasis on improving the quality of ODF using normalization and regularization [2], [3], change of basis [4]–[6], sharping deconvolution [7], compressed sensing [8], etc. Meanwhile, other quantities were also used to describe fiber orientation or crossing, including the fiber orientation distribution (FOD) from the spherical deconvolution method [9], [10], the orientation map derived from the diffusion orientation transform (DOT) based on the Fourier transform relationship between water displacement probability and diffusion-attenuated magnetic resonance (MR) signal expressed in spherical coordinates [11], and the water molecule displacement probability function [12] using the mixture of Wisharts.

The global shape information of ODFs has been compared by some quantitative measures. The mean square error[3], root-mean square error (RMSE) [5], normalized mean squared error (NMSE) [8] between the noisy ODF and the noise free ODF. The greater these metric values are, the more the noisy ODFs is different from noise free ODF. A widely adopted assumption of these metrics is that the loss of perceptual quality is directly related to the visibility of ODF. In [13], a more global description of the ODF, called Kullback-Leibler (sKL) method coming from information theory, was proposed that uses gold standard ODFs as ground-truth to assess how accurately the diffusion profile could be reconstructed from sub-sampled data based on different angular sampling schemes. The sKL method allows for the measurement of the discrepancy between the reconstructed and ground-truth ODFs. Such methods can be used for comparing ground truth ODFs and estimated ODFs. In [14], the authors used an objective criterion from statistics, called Dip test [15] that estimates the maximum distance between the empirical distribution function and the closest unimodal distribution function, to compare the quality of crossing fibers. However, the Dip test method requires sampling a direction from the ODFs to be able to perform the Dip test in a one- or two-dimensional (2D) space, and such sampling should be appropriate.

The shape and sharpness of the ODF's peaks, which reflect the local spread of fibers, and the peak anisotropy (indicating how elliptical the peak cross

section) which reflects local fiber bending or fanning [16]. However, the model proposed in [16] can only model the uncertainty in fiber orientation, the peak height is not used. Rotation invariant feature that takes the eigenvalues of spherical functions as rotation invariant metrics to describe the shape of ODFs, implies that the metric was directly dependent on the used spherical harmonic representation of HARDI signals [17]. However, the reconstruction method that represents HARDI signals in terms of other spherical basis is also proposed in [4], [6], [8].

In this study, we propose a novel paradigm to quantitatively and accurately assess ODF or other quantities by measuring their morphological characteristics. The idea consists in regarding an ODF as a three-dimensional (3D) point cloud (Figure 1), projecting the 3D point cloud onto an angle-distance map (ADM), constructing an angle-distance matrix (ADMAT), and calculating the metrics such as the length ratio, separability and uncertainty.

Figure 1: Examples of 3D point cloud representation. Left: ODF from q-ball imaging [3]. Middle: ODF from q-ball imaging within constant solid angle [14]. Right: FOD from Constrained spherical deconvolution [18].

2 3D point cloud characteristics assessment paradigm

2.1 Construction of the Angle-Distance Map (ADM)

In the representation of ODFs by 3D point clouds, each point corresponds to a vector originating from the coordination system origin. The direction and the length of the vector designate the direction and the amount of the diffusion, respectively. The difference between the 3D point cloud on the left of Figure 1 and the usual ODF visualization is that the latter is a 3D surface representation of the former. The 3D surface representation of ODFs was addressed in [1]–[3], with a variant reported in [14]. It is often expressed in spherical coordinates. Concerning 3D point clouds, we express them in Cartesian coordinates by $\vec{q} = (x, y, z)^T = q\vec{e}$. Then, a 3D point cloud can be described by a set of vectors. A vector being defined by radial distance and orientation, we introduce these two parameters to characterize the 3D point clouds. If q_m represents the maximal distance with $\vec{e}_m$ as its direction, we will then take $\vec{q}_m$ as a reference vector. From the reference vector, we construct an angle-distance map (ADM) formed of small areas delineated by radial lines spaced of $90^o / N_a$ with $N_a \in \mathbb{N}$, and circles of radius k / N_c with $k = 1,...,N_c$ and $N_c \in \mathbb{N}$, where N_c designates the number of partitions in the radial direction and N_a the number of partitions of the angle range. A small area is then the intersection of an annulus and a fan sector. The annulus is determined by $(i-1)/N_c$ and i/N_c , and the fan sector by $90(j-1)/N_a$ and $90j/N_a$. The number of small areas is determined by the choice of N_a and N_c. We now project the given vectors onto this ADM. To do this, we first calculate the angle between each vector $\vec{q}$ and the reference vector $\vec{q}_m$. Since the distance q of $\vec{q}$ to the origin is known (equal to its length), we then have the values of the angle and distance, which enables us to put the vectors in the corresponding area of ADM (Figure 2). If the maximum distance appears in two or more directions, we can choose any of them as the reference direction.

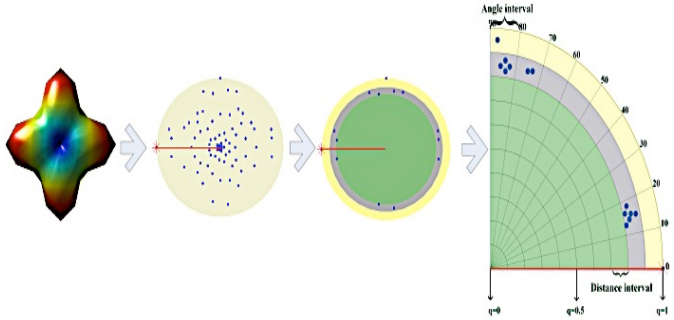

Figure 2: Projection of 3D points on the angle-distance map. From left to right: ODF, 3D point cloud with the red point indicating the reference vector, illustraton of 3D points in two annuluses, and projection of the 3D points on the ADM.

Once all the ODF points are projected on the ADM, we analyze and characterize the distribution of the projections. To this end, we first define three metrics (whose mathematical expressions will be given in Section 2.2): The length ratio that describes the main direction diffusivity, the separability that reflects the 3D point cloud's ability to separate main directions, and the uncertainty that indicates the width of the 3D point cloud's tine or peak. The definition of these metrics is illustrated in Figure 3(a). The values of the length ratio of 2-fiber range from 0 to 1, those of the separability from 0 to 1 and those of the uncertainty from 0 to $1.57\ (90\pi/180)$. The greater the length ratio is, the closer the lengths between the two fibers are. The greater the separability, the more the fibers can be easily separated. The smaller the uncertainty, the thinner the peaks of the 3D point cloud. If there are more than 2 fibers intravoxel, we will sum the values of the length ratio, separability of every 2 fibers and sum of uncertainty of each fiber.

To calculate the above metrics, we will construct the following angle-distance matrix (ADMAT).

2.2 Construction of the Angle-Distance Matrix (ADMAT) and Calculation of Morphological Criteria from ADMAT

Once all the ODF points are projected on the ADM, we analyze and characterize the distribution of the projections. To this end, we first define three metrics: The length ratio that describes the main direction diffusivity, the separability that reflects the 3D point cloud's ability to separate main directions, and the

uncertainty that indicates the width of the 3D point cloud's tine or peak. The definition of these metrics is illustrated in Figure 3(a). The values of the length ratio of 2-fiber range from 0 to 1, those of the separability from 0 to 1 and those of the uncertainty from 0 to 1.57 ($90\pi/180$). The greater the length ratio is, the closer the lengths between the two fibers are. The greater the separability, the more the fibers can be easily separated. The smaller the uncertainty, the thinner the peaks of the 3D point cloud. To construct the ADMAT, we now determine how a 3D point is projected in the corresponding small area of the ADM.

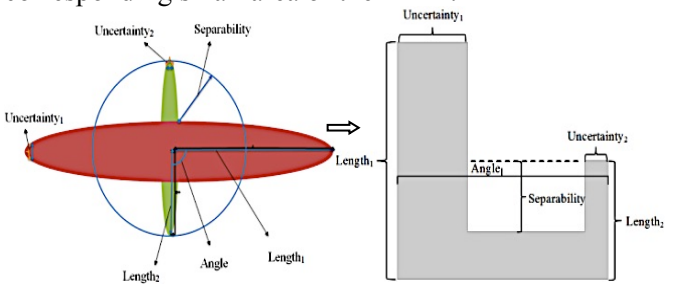

(a) (b)

Figure 3: Illustration of the definition of the length ratio, separability, and uncertainty metrics in the 3D point cloud (a) and in the schematized ADMAT (b).

We can count the number of projections of the 3D points on the area (i,j) using $N(i,j)=Card(angd(i,j))$, where $Card()$ designates the cardinal number. We then construct the ADMAT by calculating each of the elements in the area. Since the points near the origin do not contribute much to the shape of the 3D point cloud, we will attenuate their influence using

$$M_{i,j}=\sum_{p=1}^{i}a^{-(p-1)}N(p,j), \tag{1}$$

where $a>1$ is a constant. In the present study, we chose $a=10$.

From the ADMAT, we define two sets representing respectively the positions $m_{k,x}$ of zeros and the positions $n_{k,x}$ of non-zeros in the k^{th} line of ADMAT. We then, for the given k^{th} line, calculate the finite difference of $m_{k,x}$ and $n_{k,x}$ to detect discontinuous positions. $r_{k,p}$ and $v_{k,p}$ represent the set of discontinuities in $m_{k,x}$ and $n_{k,x}$, respectively. If at k^{th} line, $v_{k,p}=\varnothing$, this means that either the 3D point cloud contains only one main direction or it cannot distinguish different directions. Otherwise, at k^{th} line, the 3D point cloud contains $Card(v_k)$ main directions.

We then define an operator $fset()$ that takes a discontinuity as input and outputs a set of positions of zeros or non-zeros in the k^{th} line of ADMAT

$$fset(r_{k,p})=\begin{cases}\{m_{k,1},m_{k,2},m_{k,3}...m_{k,r_{k,1}}\}, & p=1\\ \{m_{k,r_{k,p-1}}+1,m_{k,r_{k,p-1}+1},m_{k,r_{k,p-1}+2}...m_{k,r_{k,p}}\}, & p=2,...,ls.\end{cases} \tag{2}$$

where ls designate the number of discontinuities in $m_{k,x}$ and {.} designates a set. In the same manner, we can get the set $fset(v_k)$ of positions having non-zero value.

We determine the number of lines ($\mu\times N_c$) at which two directions can be resolved, here μ is the number of lines whose $v_{k,p}$ is not empty divided by N_c. The width of the lw^{th} main direction is $\pi Nv_{\mu_1\times N_c,lw}/2N_a$ with $Card(fset(v_{\mu_1\times N_c,lw}))=Nv_{\mu_1\times N_c,lw}$, $\mu_1\times N_c$ is the line number of ADMAT at which fiber crossing is resolved for the first time. In this case, we can further determine how well the two directions can be resolved. To do that, we now compute the above-mentioned morphological metrics: length ratio $(1-\mu_1)$, separability $(\mu_{ns}-\mu_1)+1/N_c$, and uncertainty $\pi(Nv_{\mu_1\times N_c,1}+Nv_{\mu_1\times N_c,2})/4N_a$.

3 Application of morphological metrics to compare the shape of 3D point cloud

We apply the above-described morphological metrics to compare the shapes of different 3D point clouds (ODFs) derived from diffusion signals. To do that, the 3D point clouds are first reconstructed by analytical q-ball imaging (AQBI). Then the metrics such as MSE, sKL, RMSE and NMSE are calculated from 3D point clouds. Finally, we compare the quality of 3D point clouds sorted by different metrics.

The diffusion signal was simulated using the multi-tensor model. In the simulation, Rician noise was used. The signal-to-noise ratio (SNR) is defined as

$$SNR=20\times\log_{10}\left(\sqrt{\frac{\sum_{k=1}^{K}(S_k)^2}{\sum_{k=1}^{K}(S_k-SN_k)^2}}\right), \tag{3}$$

where S_k represents noise-free signal and SN_k the signal corrupted by Rician noise. The assessment was performed in the condition with b-value=3000s/mm^2 and number of diffusion gradients ND=81.

In Figure 4, the 3D point cloud of 90° crossing between 2 fibers is shown as ground truth (noise-free ODF) for the comparison of the shapes of 3D point clouds (noisy ODFs) at five voxels. For all the metrics, we observe that Voxels 1, 3, and 5 show clearer fiber crossing than Voxels 2 and 4. However, Tab 1 gives different quality sorting results of the 7 metrics. In terms of MSE, sKL and RMSE, Voxel 2 (3.2, 0.07 and 5.7) and Voxel 4 (3.4, 0.11 and 5.8) are considered of high quality, because these metrics have smaller values than Voxel 3 (4.8, 0.26 and 6.9) and Voxel 5 (4.1, 0.16 and 6.4) that show clear fiber crossing. In terms of NMSE, Voxel 1 (0.2) is the worst one of the five voxels, but it is clearly better than Voxel 2 (0.17). Our length ratio, separability and uncertainty metrics show that Voxels 1, 3 and 5 are better than Voxels 2 and 4. Each morphological metric sorted the voxels in different orders of quality based on different morphological characteristics without ground truth.

We now give the results for the 3D point clouds (obtained using AQBI) containing 3-fiber crossing each other at 90° in each voxel. As shown in Figure 5, for the ODFs (50 in total) containing 3 fibers crossing each other at 90°, the mean length ratio, mean separability and mean uncertainty are respectively 1.9, 1.7 and 1.04 in the noise-free cases. In noisy cases (SNR=10), the mean length ratio and mean separability decreased to 1.52 and 0.6 respectively, and the mean uncertainty increased to 1.7. The mean separability decreased notably by 1.1 and the uncertainty increased by 0.66 in the noisy cases.

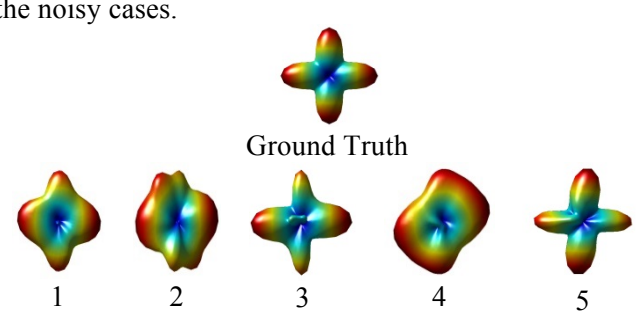

Figure 4: Examples of a noise-free 3D point cloud (ground truth) and five different 3D point clouds at 5 voxels for a SNR of 3.

Tab 1: Measurement of different shape comparison metrics of the 3D point clouds in Figure 4 and the quality of 3D point cloud sorted by metrics.

Metrics	Metric values (from left to right: Voxels 1 to 5)				
MSE x 10^7	2.0	3.2	4.8	3.4	4.1
sKL	0.07	0.07	0.26	0.11	0.16
RMSE x 10^4	4.6	5.7	6.9	5.8	6.4
NMSE	0.2	0.17	0.16	0.034	0.04
Length ratio	0.8	0	0.8	0	0.8
Separability	0.2	0	0.4	0	0.3
Uncertainty	1.1	1.57	0.69	1.57	0.87

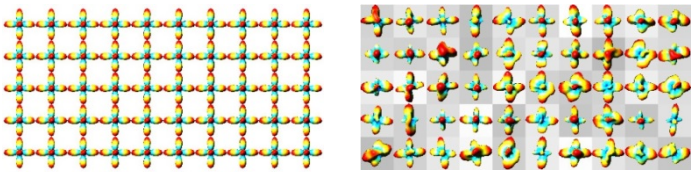

Figure 5: 3D point clouds (containing 3 fibers) computed from data noise free (left) and having SNR=10 (right) using AQBI.

4 Conclusion

We have proposed a novel paradigm allowing for the assessment of the characteristics of general 3D point clouds including the ODF in HARDI. The paradigm is based on the measurement of the morphological characteristics of 3D point clouds. The results showed that the proposed morphological metrics are consistent with the visual quality of 3D point clouds, which provides a new way to quantify their characteristics.

Acknowledgments

This work was supported by the French ANR under ANR-13-MONU-0009-01, the National Natural Science Foundation of China (61271092), International S&T Cooperation Project of China (2007DFB30320), and the Program PHC-Cai Yuanpei 2012.

References

[1] V. J. V. Wedeen, P. Hagmann, W.-Y. I. Tseng, T. G. Reese, and R. M. Weisskoff, "Mapping complex tissue architecture with diffusion spectrum magnetic resonance imaging," *Magn. Reson. Med.*, vol. 54, no. 6, pp. 1377–1386, Dec. 2005.

[2] D. S. Tuch, "Q-ball imaging," *Magn. Reson. Med.*, vol. 52, no. 6, pp. 1358–1372, Dec. 2004.

[3] M. Descoteaux, E. Angelino, S. Fitzgibbons, and R. Deriche, "Regularized, fast, and robust analytical Q-ball imaging," *Magn. Reson. Med.*, vol. 58, no. 3, pp. 497–510, Sep. 2007.

[4] O. Michailovich, Y. Rathi, and M. E. Shenton, "On Approximation of Orientation Distributions by means of Spherical Ridgelets," *IEEE Trans. image Process.*, vol. 19, no. 2, pp. 461–477, Feb. 2010.

[5] C. P. Hess, P. Mukherjee, E. T. Han, D. Xu, and D. B. Vigneron, "Q-ball reconstruction of multimodal fiber orientations using the spherical harmonic basis," *Magn. Reson. Med.*, vol. 56, no. 1, pp. 104–117, Jul. 2006.

[6] I. Kezele, M. Descoteaux, C. Poupon, F. Poupon, and J. F. Mangin, "Spherical wavelet transform for ODF sharpening," *Med. Image Anal.*, vol. 14, no. 3, pp. 332–342, 2010.

[7] M. Descoteaux, R. Deriche, T. R. Knösche, and A. Anwander, "Deterministic and probabilistic tractography based on complex fibre orientation distributions," *IEEE Trans. Med. Imaging*, vol. 28, no. 2, pp. 269–286, Feb. 2009.

[8] O. Michailovich, Y. Rathi, and S. Dolui, "Spatially Regularized Compressed Sensing for High Angular Resolution Diffusion Imaging," *IEEE Trans. Med. Imaging*, vol. 30, no. 5, pp. 1100 – 1115, May 2011.

[9] J.-D. Tournier, C.-H. Yeh, F. Calamante, K.-H. Cho, A. Connelly, and C.-P. Lin, "Resolving crossing fibres using constrained spherical deconvolution: validation using diffusion-weighted imaging phantom data.," *Neuroimage*, vol. 42, no. 2, pp. 617–625, Aug. 2008.

[10] J.-D. Tournier, F. Calamante, D. G. Gadian, and A. Connelly, "Direct estimation of the fiber orientation density function from diffusion-weighted MRI data using spherical deconvolution," *Neuroimage*, vol. 23, no. 3, pp. 1176–1185, Nov. 2004.

[11] E. Özarslan, T. Shepherd, and B. Vemuri, "Resolution of complex tissue microarchitecture using the diffusion orientation transform (DOT)," *Neuroimage*, vol. 31, no. 3, pp. 1086–1103, Jul. 2006.

[12] B. Jian, B. C. Vemuri, E. Ozarslan, P. R. Carney, and T. H. Mareci, "A novel tensor distribution model for the diffusion-weighted MR signal," *Neuroimage*, vol. 37, no. 1, pp. 164–176, Aug. 2007.

[13] L. Zhan, A. D. Leow, M. Barysheva, A. Feng, A. W. Toga, G. Sapiro, N. Harel, K. O. Lim, C. Lenglet, K. L. Mcmahon, G. I. De Zubicaray, M. J. Wright, and P. M. Thompson, "Investigating the uncertainty in multi-fiber estimation in high angular resolution diffusion imaging," in *Medical Image Computing and Computer Assisted Intervention*, pp. 256–267.

[14] I. Aganj, C. Lenglet, G. Sapiro, E. Yacoub, K. Ugurbil, and N. Harel, "Reconstruction of the Orientation Distribution Function in Single and Multiple Shell Q-Ball Imaging within Constant Solid Angle," *Magn. Reson. Med.*, vol. 64, no. 2, pp. 554–566, Aug. 2010.

[15] J. A. J. Hartigan and P. M. P. Hartigan, "The dip test of unimodality," *Ann. Stat.*, vol. 13, no. 1, pp. 70–84, Mar. 1985.

[16] K. K. Seunarine, P. a Cook, M. G. Hall, K. V Embleton, G. J. M. Parker, and D. C. Alexander, "Exploiting peak anisotropy for tracking through complex structures," *IEEE 11th Int. Conf. Comput. Vis.*, pp. 1–8, 2007.

[17] E. Schwab, H. E. Cetingül, B. Afsari, and R. Vidal, "Rotation invariant features for HARDI.," *Inf. Process. Med. Imaging*, vol. 23, no. Md, pp. 705–17, Jan. 2013.

[18] J.-D. Tournier, F. Calamante, and A. Connelly, "Robust determination of the fibre orientation distribution in diffusion MRI: non-negativity constrained super-resolved spherical deconvolution.," *Neuroimage*, vol. 35, no. 4, pp. 1459–1472, May 2007